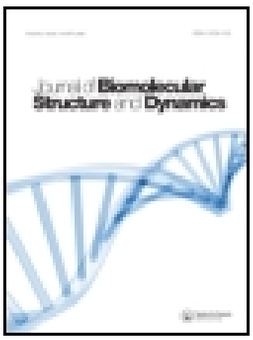

Taylor & Francis
Taylor & Francis Group

Journal of Biomolecular Structure and Dynamics

ISSN: 0739-1102 (Print) 1538-0254 (Online) Journal homepage: https://www.tandfonline.com/loi/tbsd20

Evaluation of DNA, BSA binding, DNA cleavage and antimicrobial activity of ytterbium(III) complex containing 2,2'-bipyridine ligand

Zahra Aramesh-Boroujeni, Shohreh Jahani, Mozhgan Khorasani-Motlagh, Kagan Kerman & Meissam Noroozifar

To cite this article: Zahra Aramesh-Boroujeni, Shohreh Jahani, Mozhgan Khorasani-Motlagh, Kagan Kerman & Meissam Noroozifar (2019): Evaluation of DNA, BSA binding, DNA cleavage and antimicrobial activity of ytterbium(III) complex containing 2,2'-bipyridine ligand, Journal of Biomolecular Structure and Dynamics, DOI: 10.1080/07391102.2019.1617788

To link to this article: https://doi.org/10.1080/07391102.2019.1617788

Published online: 27 May 2019.

JOURNAL OF BIOMOLECULAR STRUCTURE AND DYNAMICS
https://doi.org/10.1080/07391102.2019.1617788

Taylor & Francis
Taylor & Francis Group

Evaluation of DNA, BSA binding, DNA cleavage and antimicrobial activity of ytterbium(III) complex containing 2,2′-bipyridine ligand

Zahra Aramesh-Boroujeni[a,b], Shohreh Jahani[c], Mozhgan Khorasani-Motlagh[d], Kagan Kerman[e] and Meissam Noroozifar[d,e]

[a]Department of Clinical Laboratory, AlZahra Hospital, Isfahan University of Medical Sciences, Isfahan, Iran; [b]Department of Chemistry, University of Isfahan, Isfahan, Iran; [c]Nano Bioeletrochemistry Research Center, Bam University of Medical Sciences, Bam, Iran; [d]Department of Chemistry, University of Sistan and Baluchestan, Zahedan, Iran; [e]Department of Physical and Environmental Sciences, University of Toronto Scarborough, Toronto, Ontario, Canada

Communicated by Ramaswamy H. Sarma

ABSTRACT

In order to estimate the biological potential of a synthesized complex [$Yb(bpy)_2Cl_3.OH_2$] where bpy is 2,2′-bipyridine, its binding behavior with fish salmon-DNA (FS-DNA) and bovine serum albumin (BSA) were studied by different kinds of spectroscopy and molecular modeling methods. This complex was selected for its antibacterial and antifungal activities as well as the DNA cleavage activities were examined by agarose gel electrophoresis. The analyses of fluorescence data at four temperatures were done in order to evaluate the binding and thermodynamic parameters of the interaction of Yb(III) complex with DNA and BSA. The experimental results indicated that the major binding modes were based on groove binding with DNA and BSA. In addition, iodide quenching studies, ethidium bromide (EtBr) exclusion assay, ionic strength effect, circular dichroism, and viscosity studies reflected the binding of Yb(III) complex explicitly with the FS-DNA mainly in a groove binding mode. Moreover, molecular docking studies indicated that this complex was bound to the minor groove of DNA and to polar and apolar residues located in the subdomain IB of BSA (site 3). Also, the results of competitive experiments assessed site 3 of BSA as the most probable binding site for this complex. The molecular docking results were in good agreement with our experimental results. From both experimental and docking results, the binding constant values displayed the remarkably high affinity of Yb(III) complex to DNA as well as BSA.

ARTICLE HISTORY
Received 7 April 2019
Accepted 29 April 2019

KEYWORDS
Antibacterial activity; binding interaction; bovine serum albumin; fish salmon-DNA; molecular docking; ytterbium(III) complex

1. Introduction

In recent years, lanthanide complexes have become a very active area of research. Due to their electronic structure, long luminescence decay times, and narrow emission bands, these complexes have unusual properties that make them suitable for potential applications in lasers, catalysis, electronic and luminescent materials (Cârâc et al., 2018). In the medicinal and pharmaceutical field, lanthanide complexes have received significant attention, particularly in bioanalysis, imaging, radioimmunotherapy, fungicidal, antimicrobial and anti-tumor properties (Amoroso & Pope, 2015; Cârâc et al., 2018; Chen et al., 2011; Fricker, 2006; Kostova & Stefanova, 2010; Premkumar & Govindarajan, 2006; Thompson & Orvig, 2006). Since, lanthanide complexes indicated a variety of biological applications, several studies have investigated the binding properties of lanthanide complexes with nucleic acid and proteins such as serum albumins (Ali, Kumar, Kumar, & Pandey, 2016; Hu, Ou-Yang, Bai, Zhao, & Liu, 2010; Zhao, Sun, Ren, & Qu, 2016).

As we all know, DNA plays a vital role in the long-term storage of genetic information. DNA binding studies are very important in the development of new therapeutic reagents and DNA molecular probes. The investigation of interactions of DNA with drug molecules can help understand the molecular mechanisms of structure–activity relationships. Metal compounds can bind to DNA via covalent or noncovalent interactions (including groove, electrostatic and intercalative binding) (Shahabadi, Falsafi, & Maghsudi, 2017). Furthermore, serum albumin is the major soluble protein in all vertebrates and has many physiological functions, such as transportation, nutrition, buffering, etc (Biswas et al., 2018; Singh, Pagariya, Jain, Naik, & Kishore, 2018; Suganthi & Elango, 2019; Wang, Zhang, Zhang, Tao, & Tang, 2007; Wu et al., 2008; Yousuf, Bashir, Arjmand, & Tabassum, 2018). This inspires significant interest in the study of the biochemical behavior of lanthanide complexes including their interactions with DNA and bovine serum albumin (BSA), which are primary target molecules, when lanthanide complex is administered intravenously (Moradinia, Mansournia, Aramesh-Boroujeni, & Bordbar, 2019; Wu et al., 2008).

Here, in continuation of our previous works (Alfi, Khorasani-Motlagh, & Noroozifar, 2017; Aramesh-Boroujeni et al., 2018, 2019; Aramesh-Boroujeni, Khorasani-Motlagh, &

CONTACT Meissam Noroozifar mnoroozifar@chem.usb.ac.ir; m.noroozifar@utoronto.ca

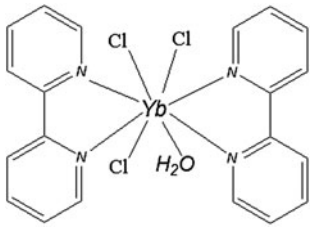

Scheme 1. Chemical structure of $[Yb(bpy)_2Cl_3(OH_2)]$.

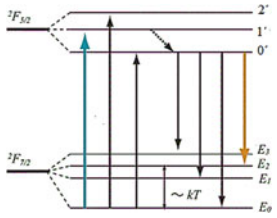

Scheme 2. Stark energy-level diagram of the $^2F_{5/2}$ and $^2F_{7/2}$ manifold of Yb(III).

Noroozifar, 2016; Jahani, Khorasani-Motlagh, & Noroozifar, 2016; Jahani, Noroozifar, Khorasani-Motlagh, Torkzadeh-Mahani, & Adeli-Sardou, 2019; Moradi, Khorasani-Motlagh, Rezvani, & Noroozifar, 2018), we attempted to introduce an Yb(III) complex that contains bpy ligand $[Yb(bpy)_2Cl_3(OH_2)]$ (Scheme 1) as a new probe to DNA and BSA. In this report, the interactions of this complex with FS-DNA and BSA have been investigated in detail by using UV–vis and fluorescence spectroscopies, circular dichroism and molecular docking method. Moreover, we have examined the DNA cleaving ability of Yb(III) complex by gel electrophoresis . In order to explore the antibacterial and antifungal effects of Yb(III) complex, minimum inhibitory concentration (MIC) and minimum bactericidal concentration (MBC) were determined against Gram-negative, Gram-positive bacteria and *Candida albicans* (*C. albicans*).

2. Experimental

2.1. Materials and instrumentations

Fish salmon DNA (FS-DNA), ethidium bromide and bovine serum albumin (BSA) were purchased from Sigma-Aldrich (Oakville, ON) and used without further purification. All other chemicals were obtained from Sigma-Aldrich (Oakville, ON) and Merck Co. (Toronto, ON). The ytterbium(III) complex was synthesized as described in our previous work (Aramesh-Boroujeni et al., 2019).

Fluorescence spectra were obtained using a Perkin Elmer, LS-3 spectrophotometer with 1.0 cm quartz cell. Electronic spectra were determined using an Analytik Jena Specord S100 spectrophotometer (Jena, Germany) with a photodiode array detector and thermostatic cell compartment. Viscosity experiments were carried out by Viscosystem® AVS 450 (Schott Instruments GmbH, Mainz, Germany) maintained at a constant temperature immersed in a thermostatic water-bath. The spectra for circular dichroism spectroscopy (CD) were collected using the JASCO-J815 (Easton, MD) at room temperature over the wavelength range 180–340 nm in a quartz cell with 1 mm path-length (Starna Cells, Atascadero, CA). The cleavage of FS-DNA was performed by Labnet International and the model of UV Transilluminator is TM-26, 15 W/302 nm UV, 230 V∼50 Hz, 1.50 Amps.

2.2. Preparation of stock solutions

All the experiments involving of interaction of Yb(III) complex with FS-DNA and BSA were carried out in deionized double-distilled water buffer containing tris(hydroxymethyl)-aminomethane (Tris, 5 mM) and sodium chloride (NaCl, 50 mM) and adjusted to pH 7.2 with hydrochloric acid. The concentration of the FS-DNA stock solution was determined spectrophotometrically by the molar extinction coefficient value (ε) of 6600 M^{-1} cm^{-1} at 260 nm. The purity of FS-DNA was checked from the absorbance ratio A_{260}/A_{280}. For FS-DNA solution, A_{260}/A_{280} greater than 1.8 showed that the FS-DNA was adequately pure and free from protein (Yu et al., 2009).

The concentration of ethidium bromide was determined by absorption spectrometry by assuming ε_{480}=5450 M^{-1} cm^{-1} and the solutions were stored in cool and dark place. Moreover, the concentration of BSA was obtained using the extinction coefficient of 44,300 M^{-1} cm^{-1} at 280 nm (Anjomshoa, Fatemi, Torkzadeh-Mahani, & Hadadzadeh, 2014). All stock solutions were stored at 4 °C and used within 4 days after preparation. The stability of ytterbium complex in aqueous solution was examined by monitoring the UV–vis spectra of the complex at various incubation times.

2.3. DNA and BSA binding experiments

The interaction of complex with FS-DNA was studied, using UV–Vis spectroscopy, in order to investigate the possible binding modes to FS-DNA and to calculate the binding constants (K_b). The DNA-binding experiments were performed at 25 °C. In this study, absorption spectrophotometric titrations were done at constant concentration of Yb(III) complex (10 μM) by increasing DNA concentrations (0–8.8 μM).

In addition, the binding interaction of the complex with DNA was studied using fluorescence spectroscopy. The fluorescence emission spectra were recorded from 300 to 500 nm at an excitation wavelength of 280 nm and the DNA-binding experiments were performed using Yb(III) complex, 0.70 μM in Tris–HCl buffer. Quenching of the emission intensity of complex at 327 nm was examined with increasing of FS-DNA concentrations from 1.1 to 15.4 μM, as a quencher. All experiments were performed at four temperatures (293, 298, 303 and 308 K).

The interaction of complex with BSA was studied using UV–vis and fluorescence spectroscopy. Absorption titrations were performed at a constant concentration of BSA (10 μM) by increasing Yb(III) complex concentrations (1.25–12.2 μM). The fluorescence titrations were performed (λ_{ex}=280, λ_{em}=347) at a constant concentration of BSA (3.0 μM) with the increasing concentrations of Yb(III) complex (0.5–6.0 μM) at four temperatures (293, 298, 303 and 308 K).

2.4. DNA cleavage studies

The DNA cleavage activity experiments with the Yb(III) complex in Tris–HCl/NaCl buffer at pH 7.2 in the absence and

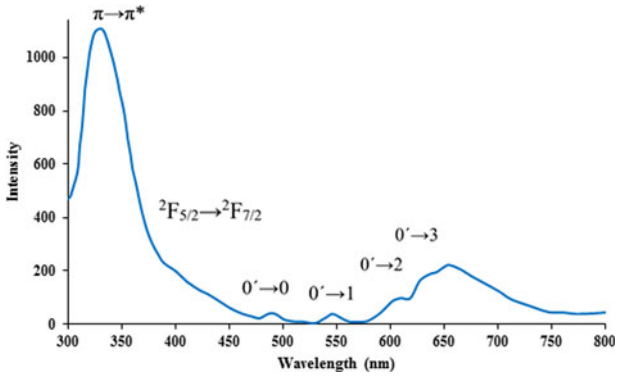

Figure 1. Emission spectrum of Yb(III) complex (1.0×10^{-3} *M*), λ_{ex}=300 nm, in acetonitrile solution at room temperature.

presence of activating agent, hydrogen peroxide (20×10^{-3} M) was monitored by agarose gel electrophoresis. All samples were incubated for 1 h at room temperature. A loading buffer (25% bromophenol blue, 0.25% xylenecyanol and 30% glycerol) was added and electrophoresis was performed for 30 min (at 100 V) and then for 15 min (at 50 V) in Tris–acetate–EDTA (TAE) buffer (40 mM Tris–base, 20 mM acetic acid, 1 mM EDTA) using 1% agarose gel containing ethidium bromide solution. The gel was stained with ethidium bromide solution at 35 °C for 15–20 min, and then destained by keeping in distilled water for 10–15 min to decrease the background. DNA bands were photographed using UV illumination at 254 nm.

2.5. Competitive experiments for BSA

In order to identify the binding site of Yb(III) complex on BSA, competitive fluorescence binding experiments have been carried out in the absence and presence of a well-defined ligand, hemin, as site-3 marker. In a typical titration experiment, the concentration of Yb(III) complex was varied from 0.5 to 6.0 μM and the concentration of BSA and hemin were kept constant at 3 and 0.3 μM, respectively. For this study, the specified amounts of the stock solution of Yb(III) complex (100 μM) were sequentially added to the BSA and BSA–hemin solutions. An excitation wavelength at 280 nm was selected, and fluorescence spectra were recorded in the range of 300–450 nm. Moreover, the absorption spectra of BSA–hemin solution in the absence and presence of Yb(III) complex (3 μM) were recorded in the range of 250–550 nm.

2.6. Docking setup

In this study, one of the best docking packages, Autodock4.2.2, was applied for docking calculations. The crystal structure of BSA (PDB ID: 3v03) and DNA duplex of sequence $d(CGCGAATTCGCG)_2$ dodecamer (PDB ID: 1BNA) were taken from Brookhaven Protein Data Bank. For the preparation of the protein input file, crystallographic water molecules were removed and missing hydrogen atoms were added to protein structures. The 3D-structure of this complex was optimized by employing the Becke-3-parameter Lee–Yang–Parr hybrid density functional theory (DFT) at the 6–31 G** basis set level by using the quantum chemistry software ORCA (Neese, 2012). For this docking, a grid map with $80 \times 80 \times 80$ points and 0.375 Å spacing were generated. Subsequently, 200 separate docking calculations were done and docking calculation consisted of maximum number of 25,000,000 energy evaluations using the Lamarckian genetic algorithm local search method (Morris et al., 1998).

2.7. Antibacterial activity

Salmonella typhi (*S. typhi*, ATCC 1609), *Pseudomonas aeruginosa* (*P. aeruginosa*, ATCC 27853), *Klebsiella pneumoniae* (*K. pneumoniae*, ATCC 10031), Methicillin-resistant *Staphylococcus aureus* (MRSA), *Escherichia coli* (*E. coli*, ATCC 25922), Vancomycin-resistant *Enterococcus* (*VRE*), *Enterococcus faecalis* (*E. faecalis*, ATCC 29212), *Acinetobacter, Enterococcus faecium* (*E. faecium*) and *Candida albicans* (*C. albicans*) were isolated from nosocomial infection. The antibacterial and antifungal activities of Yb(III) complex was estimated by the determination of the minimum inhibitory concentration (MIC) and minimum bactericidal concentration (MBC).

MIC and MBC were performed to obtain the antibacterial and antifungal spectra of Yb(III) complex using the broth dilution method (Gülçin, Kireçci, Akkemik, Topal, & Hisar, 2010; Gülçin, Küfrevioğ lu, Oktay, & Büyükokuroğ lu, 2004). Tubes containing 5 mL Mueller Hinton, supplemented with 2% glucose, broth with 10-fold dilutions of Yb(III) complex ranging from 0.005 to 45 mg L^{-1} were inoculated with 800 CFU mL^{-1} of bacteria. Test cultures were then incubated for 24 h at 37 °C, and then tubes were tested without shaking for visible turbidity. The MIC refers to the lowest complex concentrations that produced no visible turbidity. The experiments were performed three times to achieve accepted results as the MIC (μg mL^{-1}) of the strain. After the MIC has been determined, 0.1 mL of inoculum from the tubes content without visible turbidity was subcultured onto the surface of a nutrient agar plate and then incubated for 24 h at 37 °C. After the incubation period, the count of the appeared colonies on this subculture was compared to the number of CFU mL^{-1} in the original inoculum. MBC was determined as the lowest Yb(III) complex concentration allowed less than 0.1% of the original inoculum to survive.

3. Results and discussion

3.1. Luminescence properties of Yb(III) complex

Stark energy-level diagram of the $^2F_{5/2}$ and $^2F_{7/2}$ manifold of Yb(III) is given in Scheme 2 (Yu, Huang, Zhang, Lin, & Wang, 2013). The Yb(III) complex in acetonitrile exhibited luminescence characteristics of Yb(III) with obvious bands in the range of 400–700 nm and a broad band at 343 nm attributed to emission ligand. The emission spectrum of Yb(III) complex excited at 300 nm in acetonitrile is shown in Figure 1. The four emission peaks at 495, 550, 607, and 633 nm, assigned to 0′→0, 0′→1, 0′→2, and 0′→3 ($^2F_{5/2}$→$^2F_{7/2}$) transition of Yb(III) ion, respectively (Yu et al., 2013).

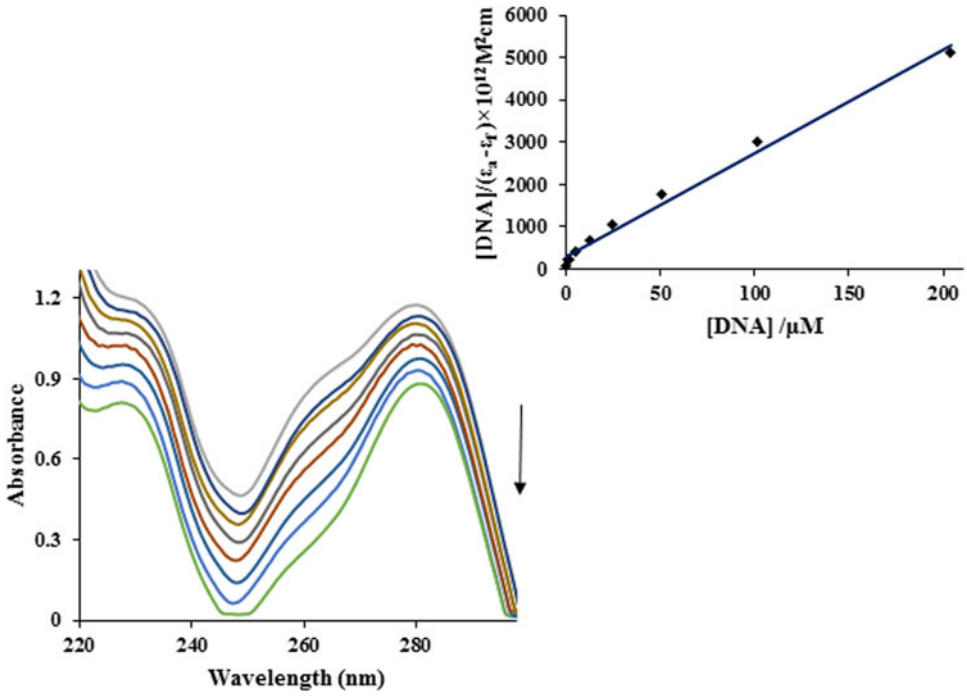

Figure 2. Absorption spectra of Yb(III) complex in the absence and in the presence of various concentrations of FS-DNA [Complex] = 1.0×10^{-5} M [DNA] = 0–8.8 μM. T = 298 K. Inset is the plot of [DNA]/(ε_a–ε_f) versus [DNA].

This characteristic emission spectrum of the Yb(III) ion confirmed that the ligand was a good chelating organic chromophore as well as can be used to absorb and transfer energy to Yb(III) ion. On the other hand, excitation of the ligand-centered emission band at 343 nm showed that the efficient energy transfer from bipyridine to the Yb(III) center did not take place and back transfer of energy from Yb(III) ion prevailed (Ferré, 2004).

3.2. DNA binding studies

3.2.1. Electronic absorption titration

In order to evaluation the DNA-binding properties of Yb(III) complex, absorption spectrophotometric titrations were done at constant concentration of this complex (10 μM) with increasing DNA concentrations (0.0–8.8 μM).

Complex binding with DNA via intercalation usually results in hypochromism together with red shift of the absorption spectra (bathochromic effect) as a result of strong interaction between complexes and the base pairs of the DNA. Instead, the hyperchromism can be observed for the groove-binding mode between complexes and DNA, if the position of the absorption spectra approximately does not change. It can be relevant with degradation of the DNA double helix structure (Mukherjee, Mondal, & Singh, 2017; Shahabadi, Hakimi, Morovati, Falsafi, & Fili, 2017).

The electronic spectra of Yb(III) complex in the absence and presence of FS-DNA are shown in Figure 2. In the presence of increasing concentrations of FS-DNA, mentioned complex exhibited decreasing with no shift of the absorption band. These results showed that the interaction of this complex and FS-DNA was in nonintercalative binding mode and could be rationalized in terms of groove-binding. The changes in absorbance with increasing of FS-DNA amount were used to evaluate the intrinsic binding constant K_b for this complex. The intrinsic binding constant, K_b, was calculated by Equation (1) (Yadav et al., 2015):

$$[Q]/(\varepsilon_a - \varepsilon_f) = [Q]/(\varepsilon_b - \varepsilon_f) + 1/K_b(\varepsilon_b - \varepsilon_f) \quad (1)$$

where ε_a, ε_f and ε_b are corresponding to the apparent extinction coefficient (A_{obsd}/[Complex]), the extinction coefficient for the free complex in solution and its completely DNA-bound form, respectively and [Q] is the concentration of FS-DNA. K_b was calculated using the plots of [DNA]/(ε_a – ε_f) versus [DNA] from the ratio of the slope to the y intercept (Figure 2). The binding constant at 298 K for Yb(III) complex was found to be 1.22×10^5 M^{-1}. The binding constant, K_b, for this complex was lower than that of the classical intercalator ethidium bromide (1.4×10^6 M^{-1}) (Chaveerach, Meenongwa, Trongpanich, Soikum, & Chaveerach, 2010). It was detected that the binding mode between Yb(III) complex and FS-DNA of (nonintercalation) changes from that of ethidium bromide (intercalation).

3.2.2. Fluorescence spectroscopic studies

The effect of complex concentration on the fluorescence intensity was investigated at the range of 10^{-3}–10^{-9} M. The results indicated that the maximum fluorescence intensity was reached when the concentration of Yb(III) complex was 7.0×10^{-7} mol L^{-1}. The influence of solvents, such as acetonitrile, methanol and water on fluorescence intensity (concentration: 7.0×10^{-7} M) was studied. The results showed that, with increasing solvent polarity (from acetonitrile to water), the emission intensity increased. Thus, in the subsequent studies, water was used as solvent.

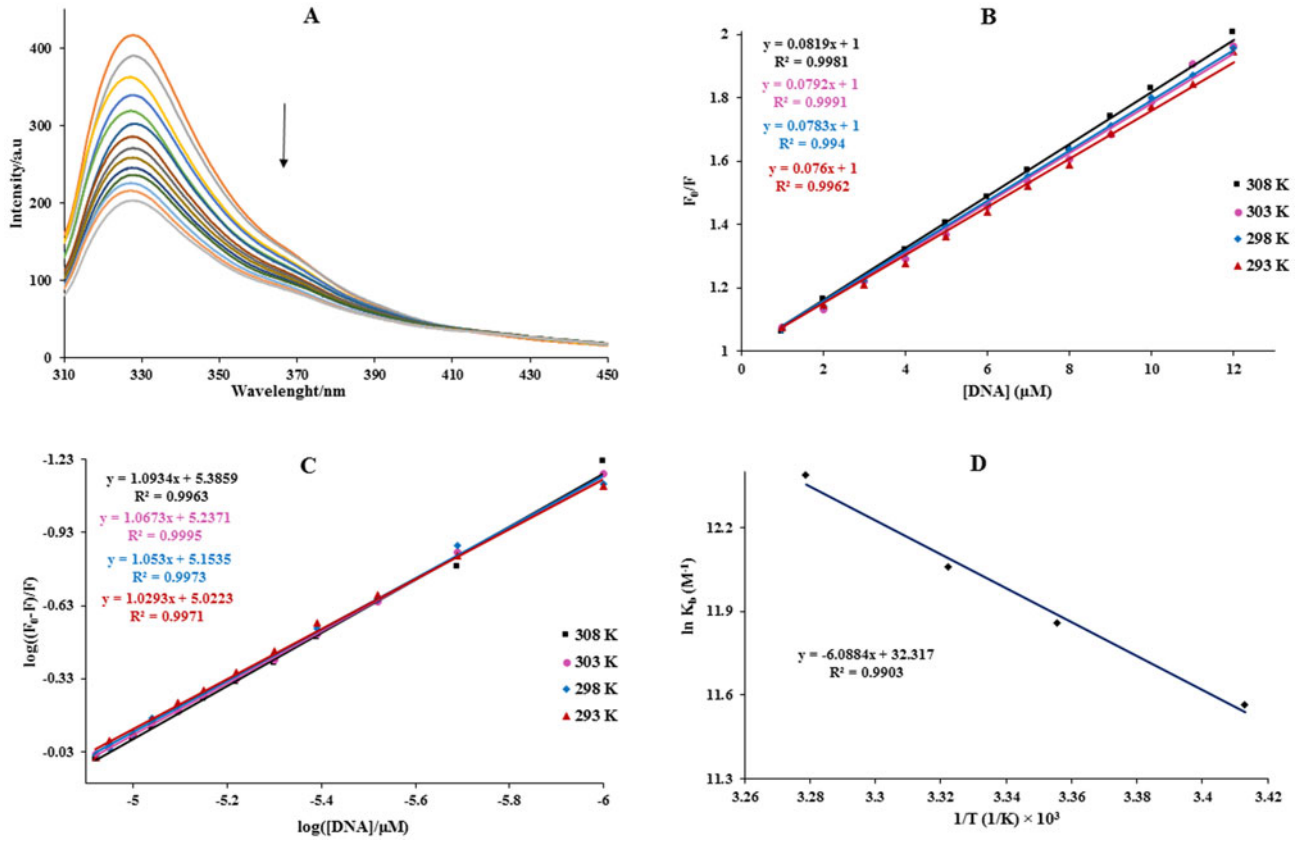

Figure 3. (A) Fluorescence emission spectra of Yb(III) complex in the absence and presence of various concentrations of FS-DNA ($T = 298$ K and λ_{ex}=280 nm). (B) Stern–Volmer curves at 293, 298, 303 and 308 K. (C) Plots of log((F_0–F)/F) versus log([DNA]/μM) for the binding of complex with DNA at 293, 298, 303 and 308 K, (D) van't Hoff plot for the binding of Yb(III) complex with DNA. The measurements were performed in Tris–HCl buffer (pH 7.2) [Complex] = 0.7 μM and [DNA] = 1.1 to 15.4 μM.

Fluorescence emission spectroscopy provides a sensitive and selective method to study the interactions between metal complexes and DNA (Rahman et al., 2017). The emission of Yb(III) complex [7.0×10^{-7} M] showed a band at 327 nm, when excited at 280 nm. The fluorescence spectra of this complex in the absence and presence of various amounts of DNA [1.1–15.4 μM] at 298 K is shown in Figure 3A.

As shown in Figure 3, the fluorescence intensity of this mentioned complex was found to be regularly decreasing with increasing concentrations of FS-DNA, which indicated the ability of FS-DNA to quench the intrinsic fluorescence of Yb(III) complex and the incidence of their binding interaction.

3.2.2.1. Quenching mechanism. Fluorescence quenching can be static quenching (the formation of a complex between quencher and fluorophore in the ground state) or dynamic quenching (a collisional process) (Aramesh-Boroujeni et al., 2016; Shahabadi, Maghsudi, Kiani, & Pourfoulad, 2011). One way to distinguish static and dynamic quenching is by investigation of the temperature on the Stern–Volmer equation (Cui, Hui, Jiang, & Zhang, 2012). Thus, temperature dependence of the fluorescence quenching measurements of Yb(III) complex–DNA binding was also determined using Stern–Volmer plots. The emission data obtained at four different temperatures (293, 298, 303 and 308 K) was analyzed by the Stern–Volmer equation (Eq. 2) (Shahabadi, Hakimi, et al., 2017):

$$\frac{F_0}{F} = 1 + K_{SV}[Q] \tag{2}$$

where F_0 and F displays the fluorescence intensities in the absence and presence of the FS-DNA, respectively, K_{SV} is the Stern–Volmer quenching constant and [Q] is the concentration of FS-DNA as quencher. Equation (2) was used to determine K_{SV} by linear regression of a plot of F_0/F versus [Q]. The values of K_{SV} for the interaction of Yb(III) complex with FS-DNA at 293, 298, 303 and 308 K were obtained, and the representative results are shown in Figure 3B with a summary in Table 1. The linear plots suggested that only one type of quenching process occurred, either in static or dynamic quenching. The results indicated that K_{SV} increased with the increase in temperature. This phenomenon proved that the possible quenching mechanism would be dynamic.

3.2.2.2. Equilibrium binding titration. The fluorescence intensities of Yb(III) complex at different concentrations of FS-DNA were analyzed by using the double logarithmic equation (Eq. 3) to calculate the binding constants (K_b) and binding sites (n) (Cui et al., 2012).

$$log\frac{F_0 - F}{F} = \log K_b + n\log[Q] \tag{3}$$

The linear equations for log ((F_0–F)/F) versus log [DNA] at different temperature values are shown in Figure 3C and the corresponding calculated parameters are summarized in Table 1.

Table 1. The Stern–Volmer constant K_{SV}, number of substantive binding sites n, the binding constant K_b and thermodynamic parameters for the binding of Yb(III) complex with DNA at different temperatures.

				$K_b \times 10^{-5}$ (M^{-1})				
Macromolecule	(K) T	$K_{SV} \times 10^{-4}$ (M^{-1})	n	UV	Fluorescence	ΔG° (kJ mol^{-1})	ΔH° (kJ mol^{-1})	ΔS° (J $mol\ K^{-1}$)
	293	7.60 ± 0.05	1.02		1.05 ± 0.04	−28.16 ± 0.04		
DNA	298	7.83 ± 0.06	1.05	4.85 ± 0.03	1.41 ± 0.02	−29.37 ± 0.05	0.05 ± 0.01	268.68 ± 0.03
	303	7.92 ± 0.04	1.06		1.72 ± 0.04	−30.37 ± 0.03		
	308	8.19 ± 0.02	1.09		2.39 ± 0.03	−31.72 ± 0.02		

The estimated values of n are close to 1 indicating that there was just a single binding site for Yb(III) complex towards FS-DNA. The K_b at 298 K for Yb(III) complex was found to be 1.41×10^5 M^{-1} similar to the value obtained using UV–Vis spectroscopy (Table 1). The values of K_b clearly underscore the remarkably high affinity of this complex to FS-DNA.

3.2.2.3. Thermodynamic studies. The interaction forces between small molecules and biomacromolecules in aqueous solution may involve van der Waals interactions, hydrophobic forces, electrostatic interactions as well as hydrogen bonds, etc. According to the data of enthalpy changes (ΔH°) and entropy change (ΔS°), the model of interaction between biomolecules similar to DNA and Yb(III) complex can be determined: (1) $\Delta H^\circ < 0$ and $\Delta S^\circ < 0$, van der Waals interactions and hydrogen bonds; (2) $\Delta H^\circ > 0$ and $\Delta S^\circ > 0$, hydrophobic forces; (3) $\Delta H^\circ < 0$ and $\Delta S^\circ > 0$, electrostatic interactions (Shahabadi & Heidari, 2014). In order to calculate enthalpy change (ΔH°) and entropy changes (ΔS°), van't Hoff equation was used (Shahabadi & Heidari, 2014).

$$\ln K_b = -\frac{\Delta G^\circ}{RT} = -\frac{\Delta H^\circ}{R}\left(\frac{1}{T}\right) + \frac{\Delta S^\circ}{R} \quad (4)$$

$$\Delta G^\circ = \Delta H^\circ - T\Delta S^\circ \quad (5)$$

The values of ΔH° and ΔS° were evaluated from the slope and intercept of the linear plot (van't Hoff equation) based on ln K versus $1/T$ (Figure 3D). The values of ΔH°, ΔS° and ΔG° between this complex with FS-DNA are listed in Table 1. As shown, the negative value of ΔG° indicated that the interaction process was spontaneous, while the positive ΔH° and ΔS° values revealed that hydrophobic forces played a main role in the binding of Yb(III) complex to FS-DNA.

3.2.3. Characterization of binding modes

3.2.3.1. Effect of the ionic strength. Monitoring the change of ionic strength is an effective method to distinguish the binding modes between small molecules and DNA. Increasing the concentration of sodium cation will increase the complexation probability between the sodium cation and DNA phosphate backbone. Due to the competition for phosphate anion, the addition of the sodium cation would weaken the surface-binding interactions, which included electrostatic interactions between small molecules and DNA (Shahabadi & Heidari, 2014; Yadav et al., 2015). To study the role of electrostatic interactions on Yb(III) complex–DNA binding, solution conditions using various concentrations of NaCl were studied. The Yb(III) complex was titrated with NaCl in the absence and presence of DNA (4.4 μM) with the increasing concentrations of NaCl concentrations from 0.05 to 0.6 M. The results indicated that the fluorescence intensity of complex–DNA system and free complex did not significantly change, which suggested nonelectrostatic binding of Yb(III) complex to FS-DNA.

3.2.3.2. Iodide quenching studies. Further support for the groove binding of Yb(III) complex with FS-DNA was obtained through KI quenching experiments. I^- ions, being negatively charged, act as well-known fluorescence quenchers for the small fluorescent molecules (Sarwar, Rehman, Husain, Ishqi, & Tabish, 2015). A highly negatively charged quencher was expected to be repelled by the negatively charged phosphate backbone of DNA, thus an intercalate molecule within the double helix should be protected from being quenched by anionic quencher. Instead, groove-binding molecules or free (unbound) aqueous complexes would be quenched readily by anionic quenchers (He, Wang, Wang, Li, & Xu, 2017). Therefore, the negatively charged I^- ion was chosen to determine the binding mode of Yb(III) complex to FS-DNA. Iodide quenching results provided a direct evidence for the groove-binding mode of our complex with FS-DNA.

Figure 4 shows the Stern–Volmer plot for fluorescence quenching of this complex by KI in the absence and presence of FS-DNA. The quenching constants (K_{SV}) of free Yb(III) complex by iodide anion was 2.80×10^4 M^{-1} and in the presence of FS-DNA, K_{SV} was 3.15×10^4 M^{-1}. It was apparent that a very little decrease in K_{SV} value was observed when this complex was bound to FS-DNA, which indicated that the bound Yb(III) complex did not intercalate between the base pairs of FS-DNA. Several reports suggested a slight protection of small fluorescent molecules by DNA even in the case of groove binding, but this protection would be significantly low as compared to intercalation (Sarwar et al., 2015). Thus, we concluded that groove-binding mode of interaction took place between our Yb(III) complex and FS-DNA.

3.2.3.3. Competitive displacement assay. In order to study further about the mode of binding between Yb(III) complex and FS-DNA, competitive binding experiments using ethidium bromide (EtBr) were also carried out. EtBr is a well-known intercalator, which is generally used as a sensitive probe to examine the mode of binding of small molecules to base pairs of DNA (Jalali & Dorraji, 2017). EtBr alone shows weak fluorescence in the aqueous solution. However, the fluorescence intensity of EtBr is significantly increased, when it intercalates into double helical DNA. Compounds having intercalative mode of binding will displace EtBr from the DNA resulting in significant decrease in fluorescence intensity of EtBr–DNA system (Jalali & Dorraji, 2017; Sarwar et al.,

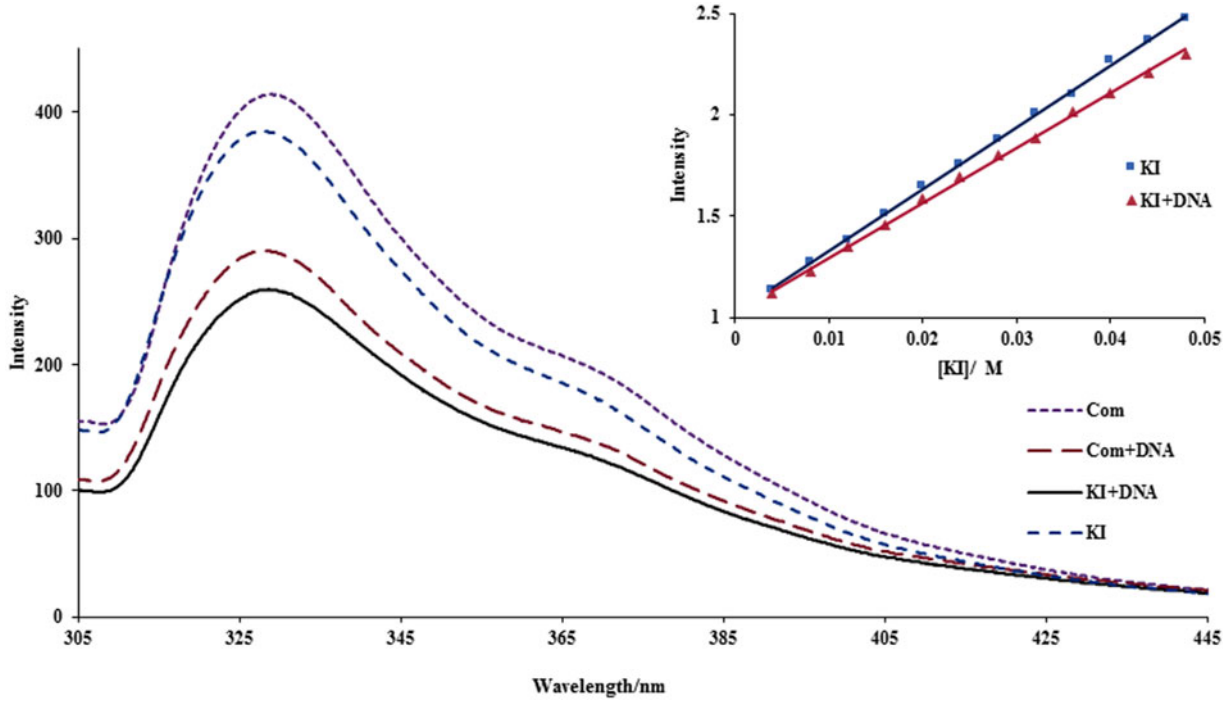

Figure 4. The fluorescence spectra of KI quenching for complex–DNA system [Complex]: 0.7 μM; [KI]: 4.0–40.0 mM. Inset is Stern–Volmer plot of the fluorescence titration data of this complex.

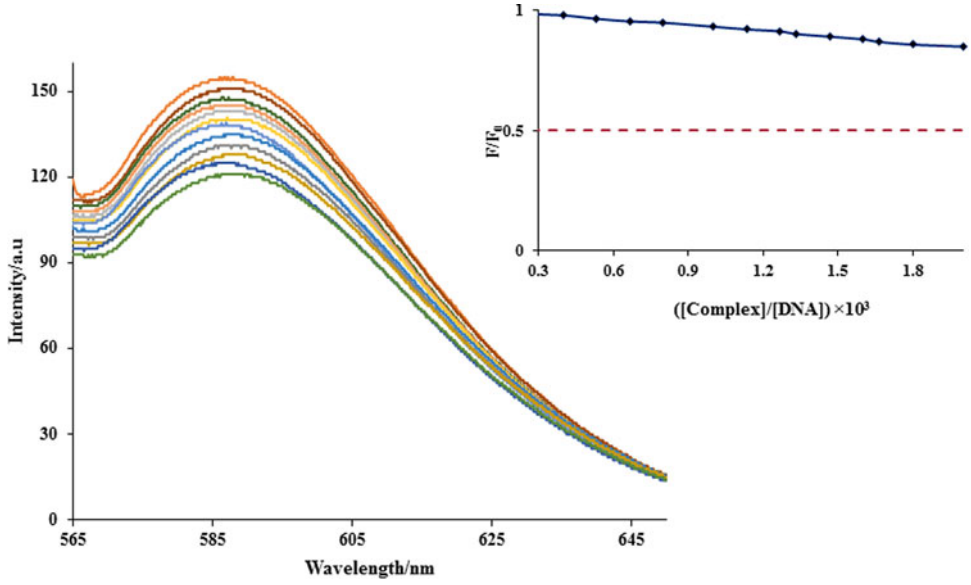

Figure 5. Fluorescence quenching curves of EtBr bound to DNA by Yb(III) complex ([EtBr] = 8.3 μM [DNA] = 140 μM [Complex] = 0–145.7 μM. Inset is the plot of F/F_0 versus [Complex]/[DNA].

2017). The effect of addition of Yb(III) complex on the fluorescence intensity of EtBr–DNA complex is shown in Figure 5. The subsequent addition of mentioned complex to EtBr–DNA system did not have any significant effect on the fluorescence intensity of EtBr–DNA system [15.2% (inset of Figure 5)] proving that the mode of binding of Yb(III) complex to FS-DNA was nonintercalative.

3.2.4. Investigation of absorption spectra

The electronic spectra of the Yb(III) complex solution in the absence and presence of FS-DNA were taken. At a wavelength of 280 nm, the absorption of Yb(III) complex and FS-DNA had partly overlapped. Their absorbance behavior satisfied the following equation:

$$A(\mathrm{FS-DNA+Yb(III)\ complex}) \approx A(\mathrm{FS-DNA}) + A(\mathrm{Yb(III)complex}) \quad (6)$$

It should be kept in mind that the absorbance spectra of both the Yb(III) complex and FS-DNA were not affected by each other, as observed in this study. Therefore, it suggested that there would be a weak interaction between Yb(III) complex and FS-DNA in nonintercalative mode (Anbu, Kamalraj, Varghese, Muthumary, & Kandaswamy, 2012).

3.2.5. Viscosity study

To further authenticate the interaction mode of Yb(III) complex and FS-DNA, viscosity measurements were performed. In the absence of crystallographic structural data, this technique was very sensitive to measure changes in the length of DNA and is regarded as the least ambiguous and the most effective method to find binding mode of DNA with metal complexes (Qais, Abdullah, Alam, Naseem, & Ahmad, 2017). A classical intercalation is expected to lengthen the DNA helix as the base pairs are separated to accommodate the binding complex, leading to substantial increase in the viscosity of DNA solution. In contrast, the groove binders and partial interacting molecules cause minor or no effect on the viscosity of DNA solution (Cui et al., 2011; Qais et al., 2017). The values of relative specific viscosity $(\eta/\eta_0)^{1/3}$ versus ([Complex]/[FS-DNA]) (where η_0 and η are the specific viscosity contributions of FS-DNA in the absence and presence of the Yb(III) complex, respectively) were plotted. The results indicated that with the increasing concentration of complex to DNA, a negligible change in the viscosity of FS-DNA was detected. From a different point of view, this result indicated that the interaction between Yb(III) complex and FS-DNA belonged to a nonintercalative binding mode (groove-binding).

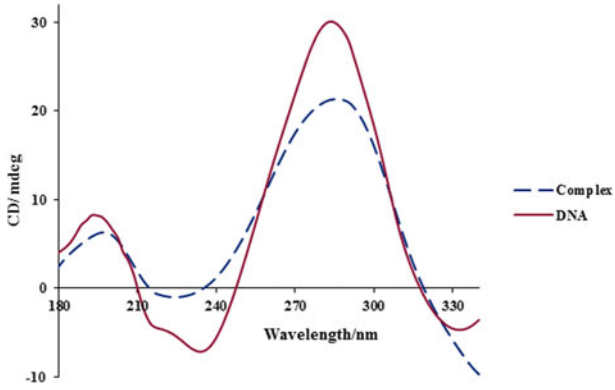

Figure 6. CD spectra of FS-DNA in the (a) absence and (b) presence the Yb(III) complex [DNA] = 5.84×10^{-3} M [Complex] = 1.0×10^{-5} M.

3.2.6. CD spectroscopy

Circular dichroism (CD) spectrophotometry has been utilized as a strong technique for exploring the chiral aspects of complexes and to provide valuable information on the mode of binding between complexes and DNA (Khan et al., 2011). Indeed, CD is useful in monitoring the conformational changes of DNA in solution. The changes in CD spectra of

Figure 7. Gel electrophoresis diagram showing the cleavage of FS-DNA (1.4×10^{-3}M) by the yttrium complex at 298 K; lane 1: DNA control; lane 1′:DNA + H_2O_2; lane 2: complex (1.2×10^{-3} M)+DNA; lane 2′:complex (1.2×10^{-3} M)+DNA + H_2O_2; lane 3: complex (2.5×10^{-3} M)+DNA; lane 3′:complex (2.5×10^{-3} M)+DNA + H_2O_2; lane 4: complex (3.7×10^{-3} M)+DNA; lane 4′: (3.7×10^{-3} M)+DNA + H_2O_2; lane 5: complex (5.0×10^{-3} M)+DNA; and lane 5′: complex (5.0×10^{-3} M)+DNA + H_2O_2.

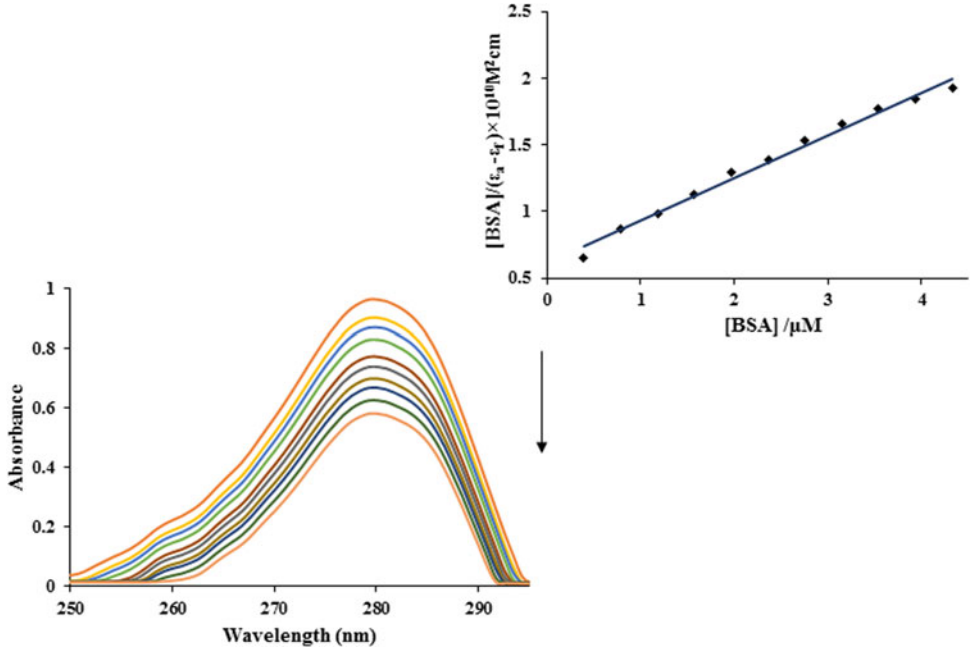

Figure 8. Absorption spectra of Yb(II) complex in the absence and presence of various concentrations of BSA [Complex] = 10 μM [BSA] = 1.25–12.2 μM. T = 298 K. Inset is the plot of [BSA]/(ε_a–ε_f) versus [BSA].

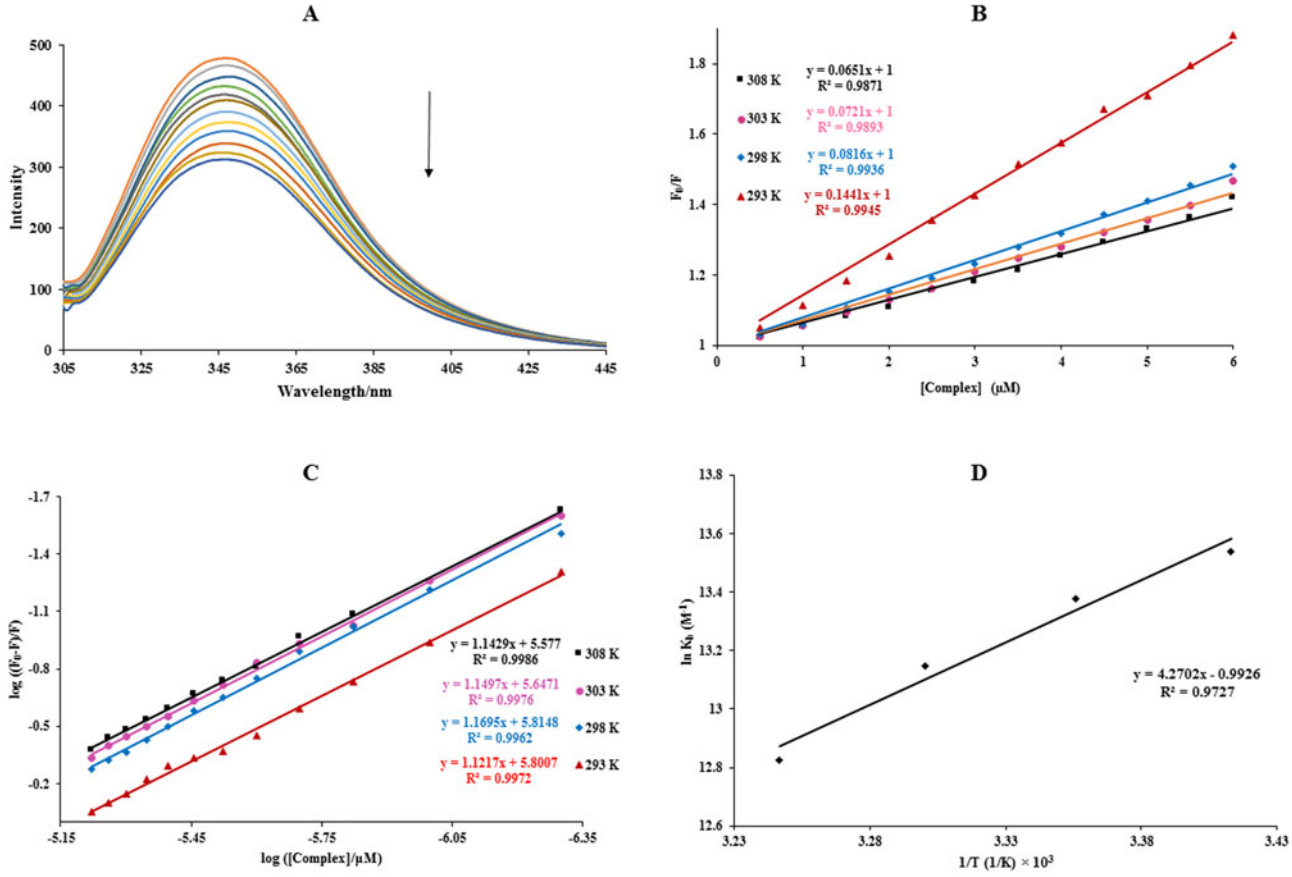

Figure 9. (A) Fluorescence emission spectra of BSA in the absence and presence of various concentrations of Yb(III) complex. (B) Stern–Volmer curves at 293, 298, 303 and 308 K. (C) Plots of $\log((F_0-F)/F)$ versus $\log([Complex]/\mu M)$ for the binding of complex with BSA at 293, 298, 303 and 308 K. (D) van't Hoff plot for the binding of Yb(III) complex with BSA ([BSA] = 3 μM and [Complex] = 0.5 to 6.0 μM, λ_{ex}=280 nm and pH = 7.2).

Table 2. The Stern–Volmer constant K_{SV}, number of substantive binding sites n, the binding constant K_b and thermodynamic parameters for the binding of Yb(II) complex with BSA at different temperatures.

				$K_b \times 10^{-5}$ (M^{-1})				
Macromolecule	(K) T	$K_{SV} \times 10^{-4}$ (M^{-1})	n	UV	Fluorescence	ΔG° (kJ mol^{-1})	ΔH° (kJ mol^{-1})	ΔS° (J $mol\ K^{-1}$)
	293	14.41 ± 0.04	1.13		7.58 ± 0.09	−32.98 ± 0.04		
BSA	298	8.16 ± 0.02	1.16	5.07 ± 0.05	6.45 ± 0.03	−33.14 ± 0.02	−35.50 ± 0.06	−8.25 ± 0.04
	303	7.21 ± 0.03	1.16		5.12 ± 0.06	−33.12 ± 0.03		
	308	6.51 ± 0.02	1.14		3.71 ± 0.07	−32.84 ± 0.05		

DNA observed on interaction with compounds can be assigned to the corresponding changes in DNA structure (Bordbar, Tabatabaee, Yeganeh Faal, Mehri Lighvan, & Fazaeli, 2015). The observed circular dichroism spectrum of FS-DNA consisted of a negative band at 235 nm due to helical geometry of B-DNA and a positive band at 289 nm due to base stacking. These bands are quite sensitive to the mode of DNA interactions with compounds. While electrostatic interaction and groove binding of compounds with DNA indicate less or no perturbations on the helicity bands and base stacking, intercalation interaction enhances the band intensities, thus stabilizing the right handed B- conformation of FS-DNA (Aramesh-Boroujeni et al., 2016; Li, Guo, Dong, Xu, & Li, 2013). The CD spectra of FS-DNA in the absence and in the presence of the Yb(III) complex are shown in Figure 6. CD spectrum of FS-DNA slightly decreased in intensity at both 235 and 289 nm bands (shifting to zero levels) after binding with this complex. This suggested that the DNA-binding of Yb(III) complex with FS-DNA induced certain conformational changes, and also reduction of base stacking. Figure 6 displayed that the conformation of FS-DNA changed due to the conversion from a more B-like to a more C-like structure within the DNA molecule. Thus, our results were indicative of a nonintercalative mode of binding of Yb(III) complex with FS-DNA and supported our hypothesis of groove-binding mode.

3.3. DNA cleavage study

Gel-electrophoresis is a valuable technique for separation of charged species (molecules) based on the migration of DNA under the influence of an electric potential (Budagumpi, Kulkarni, Kurdekar, Sathisha, & Revankar, 2010; Cankaya et al., 2007). DNA cleavage study was conducted at 298 K using ten samples of Yb(III) complex in the absence (lanes 1–5) and presence of hydrogen peroxide (20 mM, lanes 1′–5′) as an oxidant (Figure 7). In the control experiments using FS-

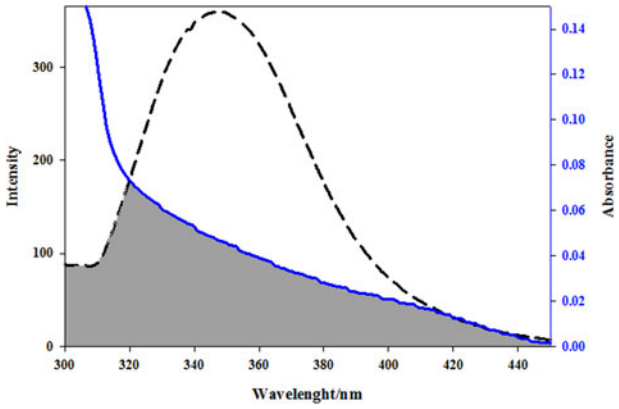

Figure 10. The overlap of the absorption spectrum (solid lines) Yb(III) complex and the fluorescence spectrum of BSA (dashed lines). The molar ratio of Yb(III) complex to BSA was 1:1.

DNA alone in the absence of this complex, no cleavages of FS-DNA were observed (lanes 1 and 1′). Lanes 2–5 and 2′-5′ represented DNA treated with increasing concentrations of Yb(III) complex, at concentrations of 1.2, 2.5, 3.7 and 5.0 mM, respectively. As shown in Figure 7, Yb(III) complex at different concentrations was able to cleave FS-DNA. However, increasing concentrations of the complex resulted in enhanced FS-DNA cleavage. Also, all complex-DNA mixtures showed a slight reduced mobility with respect to control (lanes 1 and 1′). As shown in Figure 7, the migration of DNA band reduced with increasing concentrations of Yb(III) complex (lanes 2–5 and 2′–5′). Moreover, the efficiency of DNA cleavage was higher in the presence of an oxidant (H_2O_2). This was attributed to the formation of hydroxyl radical or molecular oxygen, both of which would be capable of damaging FS-DNA through Fenton-type chemistry. Moreover, the gel image indicated that the bands had different bandwidths (smear patterns). However, with increasing concentrations of Yb(III) complex, the smear patterns were observed to increase for bands (Aramesh-Boroujeni et al., 2016).

3.4. BSA binding properties

3.4.1. UV–vis spectroscopy measurements

The efficiency of a drug is considerably influenced by the degree to which it binds to proteins in the blood plasma. UV–vis absorption spectroscopy is a significant tool to explore structural changes and complex formation in proteins (Nasir et al., 2017).

Figure 8 shows the UV–vis absorption spectra of BSA (10 μM) in the presence of Yb(III) at various concentrations (1.25–12.2 μM). The absorbance of BSA increased linearly with increasing concentration of complex along with no shift in the maximum peak position, which was an evidence for the complex formation between this complex and BSA. To determine the intrinsic binding constant, K_b, Eq. (1) used for fitting the data (Fani, Bordbar, & Ghayeb, 2013).

where in Eq.(1) [Q] is the concentration of BSA. The binding constant, K_b values for Yb(III) complex was found to be 5.07×10^5 M^{-1} (inset Figure 8). These results suggested that the interaction of Yb(III) complex with BSA was in nonintercalative binding mode and could be rationalized in terms of groove-binding mode.

Table 3. The energy transfer efficiency E, overlap integral J, the binding distance to tryptophan residue of protein r and Förster critical distance R_0 upon interaction of Yb(III) complex with BSA ([BSA] = [Yb(III) complex] = 3 μM, T = 298 K and λ_{ex} = 280 nm).

	E	J (cm^3 $Lmol^{-1}$)×10^{-14}	r (nm)	R_0 (nm)
Yb(III) complex	0.34	5.19	2.54	2.28

3.4.2. Fluorescence quenching

Fluorescence spectroscopy is a significant technique to obtain useful information on the protein–ligand interactions (Shahsavani et al., 2016). Moreover, fluorescence spectroscopy provided considerable information about the binding mechanism of ligand with protein (Nasir et al., 2017). In the presence of constant concentration of BSA (3.0 μM) while the increasing concentrations of Yb(III) complex (0.5–6.0 μM), the fluorescence spectra of BSA were obtained as shown in Figure 9A. As the data showed, the fluorescence intensity of BSA solution at 347 nm decreased regularly with the increasing concentrations of Yb(III) complex. This indicated an interaction between Yb(III) complex and BSA because of the quenching of the intrinsic fluorescence of BSA. Furthermore, no significant blue or red shifts were detected in the maximum emission wavelength of BSA suggesting that Yb(III) complex did not induce conformational changes in the structure of BSA.

In order to study the quenching process and to estimate the probable quenching mechanism, the Stern–Volmer equation was applied with Eq. (2) (Li et al., 2013). The values of K_{SV} for the interaction of BSA with our complex at different temperatures (293, 298, 303, and 308 K) were estimated as the slope of F_0/F against [Q] linear plot, and these results are shown in Figure 9B and summarized in Table 2. We could observe that there was only one type of quenching mechanism, either dynamic or static, since the Stern–Volmer plots were linear. As shown in Table 2, K_{SV} decreased with the increase in temperature, indicating that the probable quenching mechanism of the binding of Yb(III) complex to BSA was static.

3.4.2.1. Calculation of binding parameters. The binding constant (K_b) and the number of binding sites (n) were determined using Eq. (3) (Xiao et al., 2007). Figure 9C shows the double-logarithm curve and Table 2 displays the corresponding calculated parameters. The K_b for Yb(III) complex at 298 K was found to be $(6.45 \pm 0.03) \times 10^5$ M^{-1}, and the number of binding sites (n) was close to 1. The result illustrated that there was a strong binding force between Yb(III) complex and BSA, and a single binding site would be formed.

3.4.2.2. Thermodynamic parameters and nature of the binding forces. The plot of ln K_b versus $1/T$ (Figure 9D) enabled the determination of enthalpy (ΔH°), entropy (ΔS°) and free energy (ΔG°) change by using the van't Hoff equation (Eqs. 4 and 5).

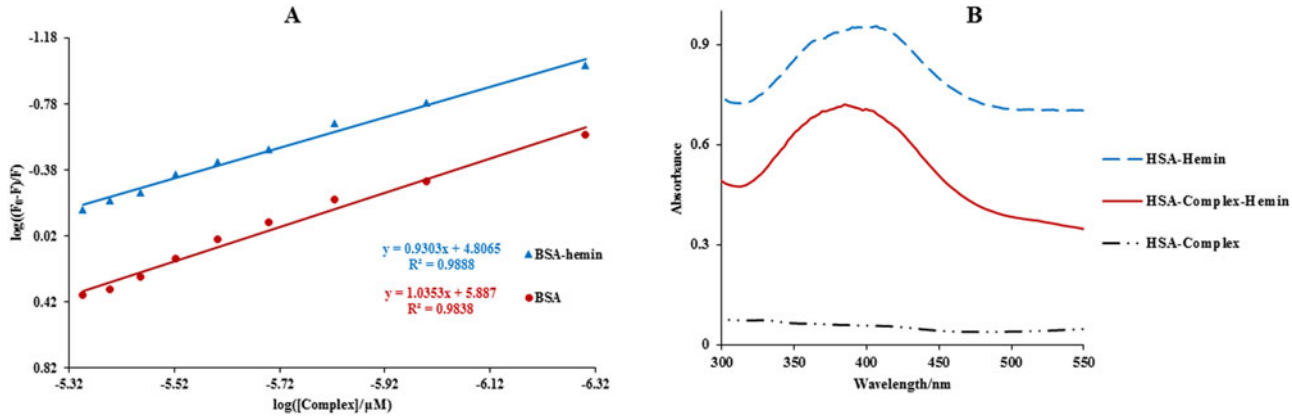

Figure 11. Effect of site marker to Yb–BSA system: (A) Plots of log((*F*$_0$–*F*)/*F*) versus log([Complex]/μM) in fluorescence study ([BSA] = 3 μM [hemin] = 0.3 μM [Yb complex] = 0.5–6.0 μM and λ_{ex}=280 nm). (B) The absorption spectra of BSA–hemin in presence and absence of Yb(III) complex [BSA] = 3 μM [hemin] = 0.3 μM and [Complex] = 3 μM.

Table 2 shows the thermodynamic parameters for the interaction of BSA with Yb(III) complex. The negative sign of ΔG° values indicated the BSA interaction process was spontaneous; the positive sign of ΔH° and ΔS° revealed that van der Waals interactions and hydrogen bonds played the main role in the binding of Yb(III) complex with BSA.

3.4.3. Energy transfer from BSA to Yb(III) complex

Fluorescence energy transfer occurs through overlapping of the emission spectrum of a fluorophore (donor, BSA) with the absorption spectrum of a molecule (acceptor, Yb(III) complex) (Buddanavar & Nandibewoor, 2017). The overlap of the absorption spectrum of this complex with the fluorescence emission spectrum of BSA is shown in Figure 10. According to the Förster's theory, the energy transfer efficiency (*E*) and the distance *r* from Yb(III) complex to BSA (Trp-214) was calculated using Eq. (7) (Yue, Zhang, Qin, & Chen, 2008):

$$E = 1 - \frac{F}{F_0} = \frac{R_0^6}{R_0^6 + r^6} \tag{7}$$

where F_0 and *F* correspond to the fluorescence intensities of BSA in the absence and presence of Yb(III) complex, *r* is the distance between BSA and this complex, and R_0 is the Förster's critical distance when the transfer efficiency is 50%, which can be given by:

$$R_0^6 = 8.79 \times 10^{-25} K^2 n^{-4} \Phi J \tag{8}$$

where K^2 is the spatial orientation factor, *n* is the refracted index of medium, Φ is the fluorescence quantum yield of BSA, and *J* is the effect of the spectral overlap integral of the fluorescence emission spectrum of donor and the absorption spectrum of acceptor and can be given by the following equation:

$$J = \frac{\sum F(\lambda)\varepsilon(\lambda)\lambda^4 \Delta\lambda}{\sum F(\lambda)\Delta\lambda} \tag{9}$$

herein, $F(\lambda)$ is the corrected emission intensity of the fluorescent donor at wavelength λ and $\varepsilon(\lambda)$ is molar absorption coefficient of acceptor at wavelength λ.

Under the experimental conditions, it has been reported that BSA would have K^2 value of 2/3, *n* of 1.336, and Φ value of 0.15 (Buddanavar & Nandibewoor, 2017). According to Eqs. (7–9), the values of *E*, *J*, R_0 and *r* were calculated and reported in Table 3. All the *R* and *r* values were in the range of 2–8 nm scale and $0.5\,R_0 < r < 1.5\ R_0$, showing a considerable interaction between this complex and BSA (Trp-214) (Hu, Liu, Zhang, Zhao, & Qu, 2005) also the occurrence of nonradiative energy transfer phenomena from BSA to Yb(III) complex with high probability.

Table 4. Binding energies and inhibition constants of investigated complex for DNA and BSA binding site.

Macromolecule	Binding energy (KCal Mol^{-1})	K_i (μM)
DNA	−6.79	10.51
BSA	−6.85	9.57

3.4.4. Competitive binding experiments with BSA

Competitive binding experiments were performed to elucidate the Yb(III) complex binding site on BSA, using hemin (subdomain IB marker), which specifically bind to BSA (Bolel, Mahapatra, & Halder, 2012; Oliveri & Vecchio, 2011). In the binding site competitive study, Yb(III) complex was regularly added to the solution of BSA and BSA–hemin mixture. After adding Yb(III) complex gradually, the fluorescence intensity of BSA linearly decreased, indicating that the bound Yb(III) complex to BSA was affected by addition of hemin. Analysis of fluorescence titration data was performed by using Eq. (3) (Figure 11A), representing the significant decrease of associative binding constant of Yb(III) complex to BSA from $7.5 \times 10^5 (M^{-1})$ to $0.63 \times 10^5 (M^{-1})$ in the presence of hemin. The competition of Yb(III) complex with hemin for occupation of the same binding site indicated that the binding of Yb(III) complex to BSA mainly located within site 3 (subdomain IB) of BSA.

To support these results, displacement studies were repeated following a different technique using absorption spectroscopy. By means of recording the changes in the absorption spectrum of Yb(III) complex bound BSA, which was performed by site marker, information about the specific binding site of Yb(III) complex in BSA molecule could be obtained. The absorption spectra of BSA–hemin solution in

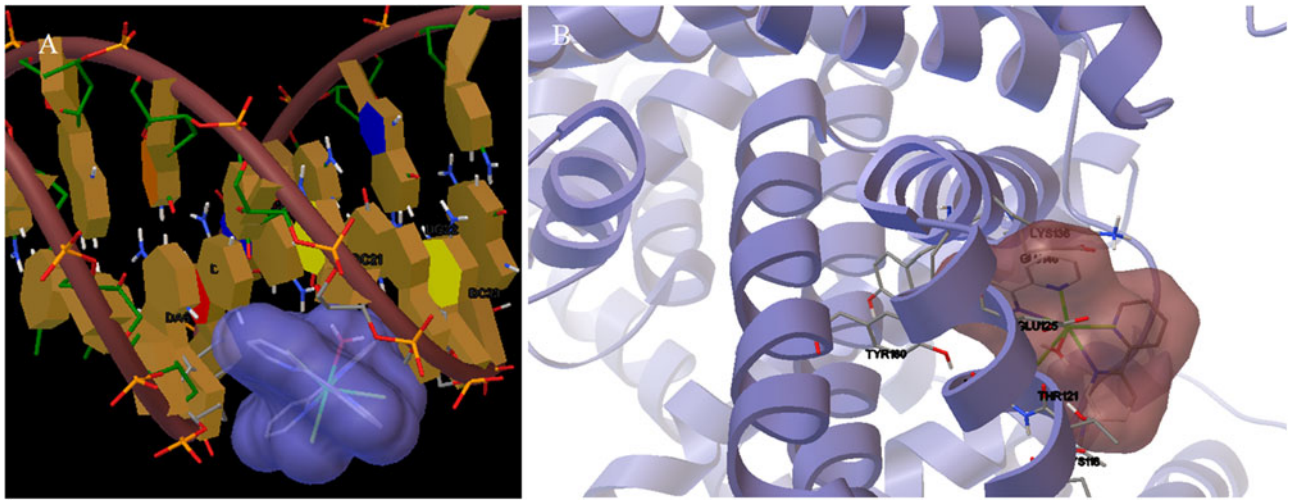

Figure 12. Detailed view of the interactions between Yb(III) complex with (A) DNA and (B) BSA.

Table 5. Antimicrobial activities of Yb(III) complex against bacteria and fungi.

Bacteria type	Bacteria or fungi	Minimum inhibitory concentrations (MIC) (μg mL^{-1})	Minimum bactericidal concentrations (MBC) (mg mL^{-1})
Gram-positive	*E. faecium*	30	1.11
	E. faecalis	15	0.55
	MRSA	30	2.22
	VRE	60	1.11
Gram-negative	*E. coli*	30	2.22
	P. aeruginosa	120	2.22
	K. pneumoniae	120	1.11
	A. baumannii	30	1.11
	S. typhi	140	1.11
Fungi	*C. albicans*	15	0.55

the absence and presence of Yb(III) complex are illustrated in Figure 11B. In the presence of Yb(III) complex, the absorption spectrum was significantly changed. From Figure 11B, the absorption of BSA–hemin solution in the presence of Yb(III) complex was significantly lower than that of without this complex in all recorded area and shifted to the spectrum of free hemin. These results also supported our hypothesis that the binding of Yb(III) complex to BSA mainly located within site 3 (subdomain IB).

3.5. Molecular docking results

3.5.1. Molecular docking with DNA

Molecular docking method take a main part in structural molecular biology and drug discovery. Binding affinity between complexes and DNA can be easily gained from molecular docking calculations. Molecular docking results indicated that Yb(III) complex had fairly appropriate binding energies (Table 4). Figure 12A revealed that Yb(III) complex approached towards the gap between DNA minor grooves mainly through bipyridine ring.

Complex was found to be best fitted in the minor groove of DNA with binding energy of –6.79 kcal mol^{-1}. The energies taken from docking method was found to be consistent with our experimental results. High negative energy predicts a strong interaction between complex and DNA as also obtained by various spectral techniques. Therefore, the docking results further strengthened our experimental findings and sustained the groove binding mode to be operational between Yb(III) complex and DNA.

3.5.2. Molecular docking with BSA

Based on RMSD, conformations were sorted into clusters and the conformations with the lowest binding energy of the largest Autodock cluster were reported. Molecular docking results illustrated that Yb(III) complex showed relatively suitable binding energies (Table 4) and bound to site 3 of BSA, which is hydrophobic with an L-shaped cavity in subdomain IB. The detailed interaction of Yb(III) complex is shown in Figure 12B. This binding site is considerably hydrophobic and Leu122, Phe133, Tyr137 and Tyr166 residues involved in hydrophobic contacts with Yb(III) complex. Moreover, this complex could establish van der Waals contacts with Lys116, Asp118, Thr121, Glu125, Lys136 and Glu140 as polar residues.

The binding free energy obtained from experimental results at 298 K for Yb(III) complex was –6.85 kcal mol^{-1}. The prediction of site 3 (subdomain IB) as the binding site of Yb(III) complex by both docking and experimental methods, was also a strong evidence for the validity of our docking calculations.

3.6. Antimicrobial and antifungal activity

The antibacterial and antifungal efficacy of Yb(III) complex against bacteria and fungi were tested based on the minimum inhibitory concentration (MIC) and minimum bactericidal concentration (MBC) methods. The MIC and MBC values of the Yb(III) complex against bacteria were 15–120 μg mL^{-1}, and 0.55–2.22 mg mL^{-1}, respectively (Table 5). The Yb(III) complex showed significant antimicrobial activity, especially against *C. albicans* and *E. faecalis*. The results in Table 5 show that Yb complex had good efficacy against different bacteria and fungi. Strong antibacterial activity was observed for the Yb(III) complex without considering gram class, including MRSA, *P. aeruginosa* and *E. coli* that are generally resistant to antibacterial compounds.

4. Conclusions

In the present study, we report a novel synthesized complex $[Yb(bpy)_2Cl_3.OH_2]$ as a probe for DNA and BSA. The FS-DNA and BSA binding properties of this complex was comprehensively studied by different kinds of spectroscopic and molecular docking examinations. The studies presented here showed the high binding affinity of this complex to DNA and BSA in addition to the strong fluorescence quenching resulted mainly from dynamic and static mechanism for DNA and BSA, respectively. Moreover, hydrophobic forces (groove binding) and van der Waals interactions played major roles in stabilizing this complex with DNA and BSA, respectively. All results that obtained from thermodynamic parameters, iodide quenching experiment, salt effect and viscosity study confirmed that Yb(III) complex could bind to FS-DNA via groove-binding mode. The results of CD spectra showed that the secondary structure of FS-DNA molecule underwent a change in the presence of Yb(III) complex. Molecular docking results for DNA displayed that Yb(III) complex had fairly appropriate binding energies and this complex approached towards the gap between DNA minor grooves.

From competitive binding experiments and molecular docking calculations, it was revealed that the binding site of this complex on BSA was in subdomain IB (site 3) and there were van der Waals interactions and hydrogen bonds between complex and residues of BSA in the binding site. The results of our molecular docking and experimental studies could be taken as a strong support for validity of docking results. From both experimental and docking results, the value of binding constant presented the remarkably high affinity of this complex to DNA and BSA. The value of resonance energy transfer and the binding distance between complex and BSA were evaluated from the analysis of Förster theory. Moreover, Yb(III) complex effectively cleaved FS-DNA in the presence and absence of H_2O_2. Further, the antimicrobial activity studies indicated that the Yb(II) complex was biologically active against different strains bacteria and the presence of the complex displayed variable growth inhibition effects on the tested bacterial strains.

The results obtained in this work can help to understand the binding mode between Yb(III) complexes with DNA and BSA, and also can provide important information about design of new inspired drugs based on the lanthanide complexes.

Funding

The financial supports of Research Councils of University of Sistan and Baluchestan, Isfahan University of Medical Sciences and Isfahan University are gratefully acknowledged. K. K. acknowledges financial support from the Canada Research Chair Tier-2 award for "Bioelectrochemistry of Proteins" (Project No. 950-231116), Ontario Ministry of Research and Innovation (Project No. 35272), Discovery Grant (Project No. 3655) from Natural Sciences and Engineering Research Council of Canada (NSERC), and Canada Foundation for Innovation (Project No. 35272).

References

Alfi, N., Khorasani-Motlagh, M., & Noroozifar, M. (2017). Evaluation DNA-/BSA-binding properties of a new europium complex containing 2, 9-dimethyl-1, 10-phenanthroline. *Journal of Biomolecular Structure & Dynamics*, *35*(7), 1518–1528. doi:10.1080/07391102.2016.1188419

Ali, M., Kumar, A., Kumar, M., & Pandey, B. N. (2016). The interaction of human serum albumin with selected lanthanide and actinide ions: Binding affinities, protein unfolding and conformational changes. *Biochimie*, *123*, 117–129. doi:10.1016/j.biochi.2016.01.012 doi:10.1016/j.biochi.2016.01.012

Amoroso, A. J., & Pope, S. J. A. (2015). Using lanthanide ions in molecular bioimaging. *Chemical Society Reviews*, *44*(14), 4723–4742. doi:10.1039/C4CS00293H

Anbu, S., Kamalraj, S., Varghese, B., Muthumary, J., & Kandaswamy, M. (2012). A series of oxyimine-based macrocyclic dinuclear zinc (II) complexes enhances phosphate ester hydrolysis, DNA binding, DNA hydrolysis, and lactate dehydrogenase inhibition and induces apoptosis. *Inorganic Chemistry*, *51*(10), 5580–5592. doi:10.1021/ic202451e

Anjomshoa, M., Fatemi, S. J., Torkzadeh-Mahani, M., & Hadadzadeh, H. (2014). DNA- and BSA-binding studies and anticancer activity against human breast cancer cells (MCF-7) of the zinc(II) complex coordinated by 5,6-diphenyl-3-(2-pyridyl)-1,2,4-triazine. *Spectrochimica Acta Part A: Molecular and Biomolecular Spectroscopy*, *127*, 511–520. doi:10.1016/j.saa.2014.02.048 doi:10.1016/j.saa.2014.02.048

Aramesh-Boroujeni, Z., Bordbar, A.-K., Khorasani-Motlagh, M., Fani, N., Sattarinezhad, E., & Noroozifar, M. (2018). Computational and experimental study on the interaction of three novel rare earth complexes containing 2, 9-dimethyl-1, 10-phenanthroline with human serum albumin. *Journal of the Iranian Chemical Society*, *15*(7), 1581–1591. doi:10.1007/s13738-018-1356-5 doi:10.1007/s13738-018-1356-5

Aramesh-Boroujeni, Z., Bordbar, A.-K., Khorasani-Motlagh, M., Sattarinezhad, E., Fani, N., & Noroozifar, M. (2019). Synthesis, characterization, and binding assessment with human serum albumin of three bipyridine lanthanide (III) complexes. *Journal of Biomolecular Structure & Dynamics*, *37*(6), 1438–1450. doi:10.1080/07391102.2018.1464959

Aramesh-Boroujeni, Z., Khorasani-Motlagh, M., & Noroozifar, M. (2016). Multispectroscopic DNA-binding studies of a terbium (III) complex containing 2, 2′-bipyridine ligand. *Journal of Biomolecular Structure & Dynamics*, *34*(2), 414–426. doi:10.1080/07391102.2015.1038585

Biswas, N., Saha, S., Khanra, S., Sarkar, A., Prasad Mandal, D., Bhattacharjee, S., … Roy Choudhury, C. (2018). Example of two novel thiocyanato bridged copper (II) complexes derived from substituted thiosemicarbazone ligand: Structural elucidation, DNA/albumin binding, biological profile analysis, and molecular docking study. *Journal of Biomolecular Structure & Dynamics*, 1–22. doi:10.1080/07391102.2018.1503564

Bolel, P., Mahapatra, N., & Halder, M. (2012). Optical spectroscopic exploration of binding of cochineal red A with two homologous serum albumins. *Journal of Agricultural & Food Chemistry*, *60*(14), 3727–3734. doi:10.1021/jf205219w

Bordbar, M., Tabatabaee, M., Yeganeh Faal, A., Mehri Lighvan, Z., & Fazaeli, R. (2015). DNA binding properties of water-soluble mixed ligand nickel (II) complex with calf-thymus DNA using different instrumental methods. *Synthesis & Reactivity in Inorganic, Metal-Organic, & Nano-Metal Chemistry*, *45*(12), 1882–1888. doi:10.1080/15533174.2014.900627

Budagumpi, S., Kulkarni, N. V., Kurdekar, G. S., Sathisha, M., & Revankar, V. K. (2010). Synthesis and spectroscopy of Co^{II}, Ni^{II}, Cu^{II} and Zn^{II} complexes derived from 3, 5-disubstituted-1H-pyrazole derivative: A special emphasis on DNA binding and cleavage studies. *European Journal of Medicinal Chemistry*, *45*(2), 455–462. doi:10.1016/j.ejmech.2009.10.026

Buddanavar, A. T., & Nandibewoor, S. T. (2017). Multi-spectroscopic characterization of bovine serum albumin upon interaction with atomoxetine. *Journal of Pharmaceutical Analysis*, *7*(3), 148–155. doi:10.1016/j.jpha.2016.10.001

Cankaya, M., Hernandez, A., Ciftci, M., Beydemir, S., Ozdemir, H., Budak, H., … Kufrevioglu, O. (2007). An analysis of expression patterns of genes encoding proteins with catalytic activities. *BMC Genomics*, *8*(1), 232. doi:10.1186/1471-2164-8-232

Cârâc, A., Boscencu, R., Dinică, R. M., Guerreiro, J. F., Silva, F., Marques, F., … Tăbăcaru, A. (2018). Synthesis, characterization and antitumor activity of two new dipyridinium ylide based lanthanide (III) complexes. *Inorganica Chimica Acta*, *480*, 83–90. doi:10.1016/j.ica.2018.05.003

Chaveerach, U., Meenongwa, A., Trongpanich, Y., Soikum, C., & Chaveerach, P. (2010). DNA binding and cleavage behaviors of

copper(II) complexes with amidino-*O*-methylurea and *N*-methyl-phenyl-amidino-*O*-methylurea, and their antibacterial activities. *Polyhedron*, *29*(2), 731–738. doi:10.1016/j.poly.2009.10.031 doi:10.1016/j.poly.2009.10.031

Chen, Z.-F., Tan, M.-X., Liu, Y.-C., Peng, Y., Wang, H.-H., Liu, H.-G., & Liang, H. (2011). Synthesis, characterization and preliminary cytotoxicity evaluation of five Lanthanide (III)–Plumbagin complexes. *Journal of Inorganic Biochemistry*, *105*(3), 426–434. doi:10.1016/j.jinorgbio.2010.12.003

Cui, F., Hui, G., Jiang, X., & Zhang, G. (2012). Interaction of 3′-azido-3′-deamino daunorubicin with DNA: Multispectroscopic and molecular modeling. *International Journal of Biological Macromolecules*, *50*(4), 1121–1126. doi:10.1016/j.ijbiomac.2012.02.007

Cui, F., Huo, R., Hui, G., Lv, X., Jin, J., Zhang, G., & Xing, W. (2011). Study on the interaction between aglycon of daunorubicin and calf thymus DNA by spectroscopy. *Journal of Molecular Structure*, *1001*(1–3), 104–110. doi:10.1016/j.molstruc.2011.06.024

Fani, N., Bordbar, A.-K., & Ghayeb, Y. (2013). Spectroscopic, docking and molecular dynamics simulation studies on the interaction of two Schiff base complexes with human serum albumin. *Journal of Luminescence*, *141*, 166–172. doi:10.1016/j.jlumin.2013.03.001

Ferré, X. M. (2004). *Crystal growth, optical characterisation and laser operation of Yb3+ in monoclinic double tungstates* [Doctoral dissertation]. Rovira i Virgili University.

Fricker, S. P. (2006). The therapeutic application of lanthanides. *Chemical Society Reviews*, *35*(6), 524–533. doi:10.1039/b509608c

Gülçin, İ., Kireçci, E., Akkemik, E., Topal, F., & Hisar, O. (2010). Antioxidant and antimicrobial activities of an aquatic plant: Duckweed (*Lemna minor* L.). *Turkish Journal of Biology*, *34*(2), 175–188.

Gülçin, İ., Küfrevioğlu, Ö. İ., Oktay, M., & Büyükokuroğlu, M. E. (2004). Antioxidant, antimicrobial, antiulcer and analgesic activities of nettle (*Urtica dioica* L.). *Journal of Ethnopharmacology*, *90*(2–3), 205–215. doi:10.1016/j.jep.2003.09.028

He, D., Wang, L., Wang, L., Li, X., & Xu, Y. (2017). Spectroscopic studies on the interactions between novel bisnaphthalimide derivatives and calf thymus DNA. *Journal of Photochemistry & Photobiology B: Biology*, *166*, 333–340. doi:10.1016/j.jphotobiol.2016.12.003 doi:10.1016/j.jphotobiol.2016.12.003

Hu, Y.-J., Liu, Y., Zhang, L.-X., Zhao, R.-M., & Qu, S.-S. (2005). Studies of interaction between colchicine and bovine serum albumin by fluorescence quenching method. *Journal of Molecular Structure*, *750*(1–3), 174–178. doi:10.1016/j.molstruc.2005.04.032

Hu, Y.-J., Ou-Yang, Y., Bai, A.-M., Zhao, R.-M., & Liu, Y. (2010). A series of novel rare earth molybdotungstosilicate heteropolyoxometalates binding to bovine serum albumin: Spectroscopic approach. *Biological Trace Element Research*, *136*(1), 8–17. doi:10.1007/s12011-009-8521-8

Jahani, S., Khorasani-Motlagh, M., & Noroozifar, M. (2016). DNA interaction of europium (III) complex containing 2, 2′-bipyridine and its antimicrobial activity. *Journal of Biomolecular Structure & Dynamics*, *34*(3), 612–624. doi:10.1080/07391102.2015.1048481

Jahani, S., Noroozifar, M., Khorasani-Motlagh, M., Torkzadeh-Mahani, M., & Adeli-Sardou, M. (2019). *In vitro* cytotoxicity studies of parent and nanoencapsulated Holmium-2, 9-dimethyl-1, 10-phenanthroline complex toward fish-salmon DNA-binding properties and antibacterial activity. *Journal of Biomolecular Structure & Dynamics*, 1–13. doi:10.1080/07391102.2018.1557077

Jalali, F., & Dorraji, P. S. (2017). Interaction of anthelmintic drug (thiabendazole) with DNA: Spectroscopic and molecular modeling studies. *Arabian Journal of Chemistry*, *10*, S3947–S3954. doi:10.1016/j.arabjc.2014.06.001 doi:10.1016/j.arabjc.2014.06.001

Khan, N-U. H., Pandya, N., Prathap, K. J., Kureshy, R. I., Abdi, S. H. R., Mishra, S., & Bajaj, H. C. (2011). Chiral discrimination asserted by enantiomers of Ni (II), Cu (II) and Zn (II) Schiff base complexes in DNA binding, antioxidant and antibacterial activities. *Spectrochimica Acta Part A: Molecular & Biomolecular Spectroscopy*, *81*(1), 199–208. doi:10.1016/j.saa.2011.06.002

Kostova, I., & Stefanova, T. (2010). Synthesis, characterization and cytotoxic/cytostatic activity of La (III) and Dy (III) complexes. *Journal of Trace Elements in Medicine & Biology*, *24*(1), 7–13. doi:10.1016/j.jtemb.2009.06.004

Li, L., Guo, Q., Dong, J., Xu, T., & Li, J. (2013). DNA binding, DNA cleavage and BSA interaction of a mixed-ligand copper(II) complex with taurine Schiff base and 1,10-phenanthroline. *Journal of Photochemistry & Photobiology: B, Biology*, *125*, 56–62. doi:10.1016/j.jphotobiol.2013.05.007

Moradi, Z., Khorasani-Motlagh, M., Rezvani, A. R., & Noroozifar, M. (2018). Evaluation of DNA, BSA binding, and antimicrobial activity of new synthesized neodymium complex containing 2,9-dimethyl 1,10-phenanthroline. *Journal of Biomolecular Structure & Dynamics*, *36*(3), 779–794. doi:10.1080/07391102.2017.1288170

Moradinia, E., Mansournia, M., Aramesh-Boroujeni, Z., & Bordbar, A. K. (2019). New transition metal complexes of 9, 10-phenanthrenequinone *p*-toluyl hydrazone Schiff base: Synthesis, spectroscopy, DNA and HSA interactions, antimicrobial, DFT and docking studies. *Applied Organometallic Chemistry*, *33*(5), e4893. doi:10.1002/aoc.4893 doi:10.1002/aoc.4893

Morris, G. M., Goodsell, D. S., Halliday, R. S., Huey, R., Hart, W. E., Belew, R. K., & Olson, A. J. (1998). Automated docking using a Lamarckian genetic algorithm and an empirical binding free energy function. *Journal of Computational Chemistry*, *19*(14), 1639–1662. doi:10.1002/(SICI)1096-987X(19981115)19:14<1639::AID-JCC10>3.0.CO;2-B

Mukherjee, A., Mondal, S., & Singh, B. (2017). Spectroscopic, electrochemical and molecular docking study of the binding interaction of a small molecule 5H-naptho [2, 1-f][1, 2] oxathieaphine 2, 2-dioxide with calf thymus DNA. *International Journal of Biological Macromolecules*, *101*, 527–535. doi:10.1016/j.ijbiomac.2017.03.053

Nasir, Z., Shakir, M., Wahab, R., Shoeb, M., Alam, P., Khan, R. H. … Lutfullah, (2017). Co-precipitation synthesis and characterization of Co doped SnO_2 NPs, HSA interaction via various spectroscopic techniques and their antimicrobial and photocatalytic activities. *International Journal of Biological Macromolecules*, *94*, 554–565. doi:10.1016/j.ijbiomac.2016.10.057

Neese, F. (2012). The ORCA program system. *Wiley Interdisciplinary Reviews: Computational Molecular Science*, *2*(1), 73–78. doi:10.1002/wcms.81

Oliveri, V., & Vecchio, G. (2011). A novel artificial superoxide dismutase: Non-covalent conjugation of albumin with a Mn III salophen type complex. *European Journal of Medicinal Chemistry*, *46*(3), 961–965. doi:10.1016/j.ejmech.2010.12.023

Premkumar, T., & Govindarajan, S. (2006). Antimicrobial study on trivalent lighter rare-earth complexes of 2-pyrazinecarboxylate with hydrazinium cation. *World Journal of Microbiology & Biotechnology*, *22*(10), 1105–1108. doi:10.1007/s11274-006-9149-x

Qais, F. A., Abdullah, K., Alam, M. M., Naseem, I., & Ahmad, I. (2017). Interaction of capsaicin with calf thymus DNA: A multi-spectroscopic and molecular modelling study. *International Journal of Biological Macromolecules*, *97*, 392–402. doi:10.1016/j.ijbiomac.2017.01.022

Rahman, Y., Afrin, S., Husain, M. A., Sarwar, T., Ali, A., & Tabish, M. (2017). Unravelling the interaction of pirenzepine, a gastrointestinal disorder drug, with calf thymus DNA: An *in vitro* and molecular modelling study. *Archives of Biochemistry & Biophysics*, *625*, 1–12. doi:10.1016/j.abb.2017.05.014[Mismatch]

Sarwar, T., Ishqi, H. M., Rehman, S. U., Husain, M. A., Rahman, Y., & Tabish, M. (2017). Caffeic acid binds to the minor groove of calf thymus DNA: A multi-spectroscopic, thermodynamics and molecular modelling study. *International Journal of Biological Macromolecules*, *98*, 319–328. doi:10.1016/j.ijbiomac.2017.02.014 doi:10.1016/j.ijbiomac.2017.02.014

Sarwar, T., Rehman, S. U., Husain, M. A., Ishqi, H. M., & Tabish, M. (2015). Interaction of coumarin with calf thymus DNA: Deciphering the mode of binding by *in vitro* studies. *International Journal of Biological Macromolecules*, *73*, 9–16. doi:10.1016/j.ijbiomac.2014.10.017

Shahabadi, N., Falsafi, M., & Maghsudi, M. (2017). DNA-binding study of anticancer drug cytarabine by spectroscopic and molecular docking techniques. *Nucleosides, Nucleotides & Nucleic Acids*, *36*(1), 49–65. doi:10.1080/15257770.2016.1218021

Shahabadi, N., Hakimi, M., Morovati, T., Falsafi, M., & Fili, S. M. (2017). Experimental and molecular modeling studies on the DNA-binding of diazacyclam-based acrocyclic copper complex. *Journal of Photochemistry & Photobiology B: Biology*, *167*, 7–14. doi:10.1016/j.jphotobiol.2016.12.023

Shahabadi, N., & Heidari, L. (2014). Synthesis, characterization and multi-spectroscopic DNA interaction studies of a new platinum complex containing the drug metformin. *Spectrochimica Acta Part A: Molecular & Biomolecular Spectroscopy*, *128*, 377–385. doi:10.1016/j.saa.2014.02.167

Shahabadi, N., Maghsudi, M., Kiani, Z., & Pourfoulad, M. (2011). Multispectroscopic studies on the interaction of 2-tert-butylhydroquinone (TBHQ), a food additive, with bovine serum albumin. *Food Chemistry*, *124*(3), 1063–1068. doi:10.1016/j.foodchem.2010.07.079

Shahsavani, M. B., Ahmadi, S., Aseman, M. D., Nabavizadeh, S. M., Alavianmehr, M. M., & Yousefi, R. (2016). Comparative study on the interaction of two binuclear Pt (II) complexes with human serum albumin: Spectroscopic and docking simulation assessments. *Journal of Photochemistry & Photobiology B: Biology*, *164*, 323–334. doi:10.1016/j.jphotobiol.2016.09.035

Singh, N., Pagariya, D., Jain, S., Naik, S., & Kishore, N. (2018). Interaction of copper (II) complexes by bovine serum albumin: Spectroscopic and calorimetric insights. *Journal of Biomolecular Structure & Dynamics*, *36*(9), 2449–2462. doi:10.1080/07391102.2017.1355848

Suganthi, M., & Elango, K. P. (2019). Spectroscopic and molecular docking studies on the albumin-binding properties of metal (II) complexes of Mannich base derived from lawsone. *Journal of Biomolecular Structure & Dynamics*, *37*(5), 1136–1145. doi:10.1080/07391102.2018.1450788

Thompson, K. H., & Orvig, C. (2006). Editorial: Lanthanide compounds for therapeutic and diagnostic applications. *Chemical Society Reviews*, *35*(6), 499. doi:10.1039/b606622b

Wang, Y.-Q., Zhang, H.-M., Zhang, G.-C., Tao, W.-H., & Tang, S.-H. (2007). Interaction of the flavonoid hesperidin with bovine serum albumin: A fluorescence quenching study. *Journal of Luminescence*, *126*(1), 211–218. doi:10.1016/j.jlumin.2006.06.013

Wu, S.-S., Yuan, W.-B., Wang, H.-Y., Zhang, Q., Liu, M., & Yu, K.-B. (2008). Synthesis, crystal structure and interaction with DNA and HSA of (*N*,*N*′-dibenzylethane-1, 2-diamine) transition metal complexes. *Journal of Inorganic Biochemistry*, *102*(11), 2026–2034. doi:10.1016/j.jinorgbio.2008.08.005

Xiao, J. B., Chen, J. W., Cao, H., Ren, F. L., Yang, C. S., Chen, Y., & Xu, M. (2007). Study of the interaction between baicalin and bovine serum albumin by multi-spectroscopic method. *Journal of Photochemistry & Photobiology A: Chemistry*, *191*(2–3), 222–227. doi:10.1016/j.jphotochem.2007.04.027

Yadav, S., Yousuf, I., Usman, M., Ahmad, M., Arjmand, F., & Tabassum, S. (2015). Synthesis and spectroscopic characterization of diorganotin (iv) complexes of *N*′-(4-hydroxypent-3-en-2-ylidene) isonicotinohydrazide: Chemotherapeutic potential validation by *in vitro* interaction studies with DNA/HSA, DFT, molecular docking and cytotoxic activity. *RSC Advances*, *5*(63), 50673–50690. doi:10.1039/C5RA06953J

Yousuf, I., Bashir, M., Arjmand, F., & Tabassum, S. (2018). Multispectroscopic insight, morphological analysis and molecular docking studies of CuII-based chemotherapeutic drug entity with human serum albumin (HSA) and bovine serum albumin (BSA). *Journal of Biomolecular Structure & Dynamics*, 1–15. doi:10.1080/07391102.2018.1512899

Yu, H.-J., Huang, S.-M., Li, L.-Y., Jia, H.-N., Chao, H., Mao, Z.-W., … Ji, L.-N. (2009). Synthesis, DNA-binding and photocleavage studies of ruthenium complexes $[Ru(bpy)_2(mitatp)]^{2+}$ and $[Ru(bpy)_2(nitatp)]^{2+}$. *Journal of Inorganic Biochemistry*, *103*(6), 881–890. doi:10.1016/j.jinorgbio.2009.03.005

Yu, Y., Huang, Y., Zhang, L., Lin, Z., & Wang, G. (2013). Growth and spectral assessment of Yb^{3+}-doped $KBaGd(MoO_4)_3$ crystal: A candidate for ultrashort pulse and tunable lasers. *PloS one*, *8*(1), e54450. doi:10.1371/journal.pone.0054450

Yue, Y., Zhang, Y., Qin, J., & Chen, X. (2008). Study of the interaction between esculetin and human serum albumin by multi-spectroscopic method and molecular modeling. *Journal of Molecular Structure*, *888*(1–3), 25–32. doi:10.1016/j.molstruc.2007.11.028

Zhao, C., Sun, Y., Ren, J., & Qu, X. (2016). Recent progress in lanthanide complexes for DNA sensing and targeting specific DNA structures. *Inorganica Chimica Acta*, *452*, 50–61. doi:10.1016/j.ica.2016.04.014